Triangular Elastomeric Stamps for Optical Applications: Near-Field Phase Shift Photolithography, 3D Proximity Field Patterning, Embossed Antireflective Coatings, and SERS Sensing

*Audrey M. Bowen, Michael J. Motala, J. Matthew Lucas, Sidhartha Gupta, Alfred J. Baca, Agustin Mihi, A. Paul Alivisatos, Paul V. Braun, and Ralph G. Nuzzo**

The use of a decal transfer lithography technique to fabricate elastomeric stamps with triangular cross-sections, specifically triangular prisms and cones, is described. These stamps are used in demonstrations for several prototypical optical applications, including the fabrication of multiheight 3D photoresist patterns with near zero-width features using near-field phase shift lithography, fabrication of periodic porous polymer structures by maskless proximity field nanopatterning, embossing thin-film antireflection coatings for improved device performance, and efficient fabrication of substrates for surface-enhanced Raman spectroscopic sensing. The applications illustrate the utility of the triangular poly(dimethylsiloxane) decals for a wide variety of optics-centric applications, particularly those that exploit the ability of the designed geometries and materials combinations to manipulate light–matter interactions in a predictable and controllable manner.

1. Introduction

A number of lithography techniques that expand upon traditional semiconductor fabrication have recently been described in the literature, specifically in the realm of 3D patterning. Of particular interest in these developments are ones that enable low cost, high throughput, fabrication schemes for the diverse form of functional structures required for electronic and optical applications. Some notable examples of techniques motivated by topics attracting significant attention in current research include nanoimprint lithography,[1,2] nanosphere lithography,[3,4] scanning probe lithography techniques,[5,6] and advanced forms of soft lithography,[7–10] including interference lithography with elastomeric contact masks.[11–13] Additionally, the realization of structures with triangular cross-sections, such as cones and prisms, would enable applications in microfluidic lab-on-a-chip devices,[14,15] optical components, antireflective coatings,[16,17] self-cleaning surfaces with tuned contact angles,[18–20] surface enhanced Raman spectroscopy (SERS) sensing,[21,22] and probe-based patterning techniques.[23,24] A number of useful fabrication techniques have been developed to achieve this geometrical attribute, most commonly relying on etching to define the patterns. The most commonly used method uses KOH-based anisotropic wet etching of Si(100) patterned with photoresist lines, to etch along the <110> direction and thus form an array of linear pits with isosceles triangle shaped cross-sections.[25–28] The feature pitch is dictated by the precision of the alignment of the photoresist features

A. M. Bowen, M. J. Motala, Prof. R. G. Nuzzo
Department of Chemistry
Frederick Seitz Materials Research Laboratory
University of Illinois at Urbana-Champaign
Urbana, IL 61801, USA
E-mail: r-nuzzo@illinois.edu

J. M. Lucas
Department of Mechanical Engineering
University of California at Berkeley
Berkeley, CA 94720, USA

S. Gupta, Prof. P. V. Braun
Department of Materials Science and Engineering
Frederick Seitz Materials Research Laboratory
University of Illinois at Urbana-Champaign
Urbana, IL 61801, USA

Dr. A. J. Baca
U.S. Navy NAVAIR-NAWCWD
Research and Intelligence Department
Chemistry Branch
China Lake, CA 93555, USA

A. Mihi
Beckman Institute for Advanced Science and Technology
University of Illinois at Urbana-Champaign
Urbana, IL 61801, USA

Prof. A. P. Alivisatos
Department of Chemistry
University of California at Berkeley
Materials Sciences Division
Lawrence Berkeley National Laboratory
Berkeley, CA 94720, USA

DOI: 10.1002/adfm.201102455

with respect to the <110> direction, as well as etch time. Perfect alignment will produce features with no horizontal space between them, with misalignment leading to a variable spacing between them. Sample to sample variations are problematic unless complicated pre-etch fiduciary markers are used to sustain a precise wafer alignment.

Advanced soft lithography techniques have enabled alternative fabrication schemes that can achieve patterning of 3D features without relying on traditional etching protocols. For example, when a flat unpatterned poly(dimethylsiloxane) (PDMS) sheet is pre-strained and then exposed to a UV-ozone treatment, a thin silica film forms on the PDMS surface. Upon release of the strain, the PDMS sheet will wrinkle in a manner that produces periodic sinusoidal grooves in the material.[29–31] To fabricate sharper, triangular grooves in the material, the PDMS is first subject to UV-ozone treatment, and then a uniaxial strain is applied that selectively cracks the silica surface in a regular linear pattern and subsequently initiates ripping of the underlying PDMS to form triangular grooves.[32] While this approach provides a promising method for realizing sub-micron triangular channels, the resulting feature widths, aspect ratios, and actual pattern arrangements are limited in scope, and the process variables are difficult to control due to the nature of the fabrication process.

In addition to triangular prisms, cone-shaped features have been achieved through nanosphere lithography and similar etching-based protocols that exploit self-assembled colloidal spheres as the etch mask.[3,4,19] The size of the colloids used will dictate the resulting size and spacing of the cones; requiring the processing of new colloidal masks whenever a new design rule is desired. While this technique does provide a means for large pattern areas, there are also obvious limitations in terms of the spatial layout and fidelity of the resulting cones, as the formation of the etch mask relies solely on the lowest energy configuration achieved by the colloids (and their embedded defects) during the self-assembly process. This restricts the designs for specific patterns of cones that can be accomodated. Alternatively, direct writing approaches such as electron-beam lithography and focused ion beam milling have been demonstrated for shaping of micro- and nanoscale 3D features.[33] This type of patterning scheme, while minimizing constraints on the resulting shape of the features fabricated, has significant limitations in terms of mass production and large area patterning due to the serial nature of the processing.

The present work describes the development of new soft-lithographic patterning capabilities, ones exploiting competencies of soft triangular stamp design within a range of applications that direct light-matter interactions to achieve useful forms of materials patterning. The fabrication protocols described here are based on variants of decal transfer lithography that produce PDMS features with inherently triangular cross-sections.[34] These printed patterns are then used as soft lithography masters to form elastomeric stamps used to transfer the desired surface topography into application-enabling materials. Adapting soft lithography protocols such as these to make polymer based soft lithography masters is advantageous as it provides a quicker and easier route, as well as a more diverse range of achievable pattern layouts, than the more conventional silicon etching approach. The 3D patterned stamps are used to fabricate patterns in photoresist approaching zero-width by near field phase shift lithography, periodic porous structures in polymer by proximity field nanopatterning, embossed inorganic antireflective coatings for optical devices, and SERS substrates for molecular detection.

2. Results and Discussion

2.1. Stamp Fabrication by Decal Transfer Lithography

In this paper, two fabrication techniques based on established variants of decal transfer lithography[34,35] are used to print triangular PDMS features onto substrates that can then function as high resolution soft lithography masters.[36,37] The first scheme (herein referred to as Method I) is unique in its ability to print PDMS decals from a flat PDMS stamp, eliminating the need for a soft lithography master to predefine features.[34] As described in **Figure 1**a–e, the enabling master for this process is a special UV-ozone mask that contains lithographically defined micro-reactor chambers. This mask isolates the production of reactive oxygen species to desired areas, by forming selective conformal contact with the surface of the PDMS; the micro-reactor chambers are of sufficient volume that enough oxygen is trapped to activate the PDMS surface via a UV-ozone exposure. When the locally activated PDMS face is brought into intimate contact with a hydroxylated substrate (i.e., SiO_2 treated with pirhana solution), adhesive bonds form between the activated regions of the PDMS and the substrate. After heating, the PDMS stamp is slowly peeled from the receiving substrate, leaving behind PDMS decals in a pattern dictated by the UV-ozone mask. The printed PDMS has characteristically triangular cross-sections that result from the cohesive failure into the bulk of the polymer that is initiated at the edge of the pre-defined features. The resulting shape of the PDMS depends on the UV-ozone mask pattern; cones form when a mask containing open circular holes are used, while triangular prisms form from line patterns. We have found that the cohesive failure of the PDMS is dependent on the direction and nature of the applied peeling force, and as a result the printed cones are slightly asymmetrical. The aspect ratio of the features is directly correlated to the lateral feature size, maintaining a height to width ratio of approximately 0.3. Minimum feature size is, as far as we have seen through experiments, largely limited by the ability to perform the photolithography step needed to fabricate the UV-ozone mask. Preliminary experiments conducted by our group using high resolution lithography to achieve sub-micrometer patterns, specifically phase-shift lithography and electron-beam lithography, have enabled printing of PDMS decals with lateral width of 700 nm. Below this, the printed decals seem to degrade in integrity and do not exhibit uniform feature heights.

An alternative process (Method II) circumvents much of the difficulty associated with using Method I to print higher resolution features, specifically those that are below the resolution limit of traditional i-line lithography.[34] For this fabrication scheme, existing high resolution soft lithography masters used by our group to fabricate nanostructured plasmonic crystals[38–40] were adopted to produce PDMS stamps containing arrays of cylindrical posts. It is important to note that soft lithography masters

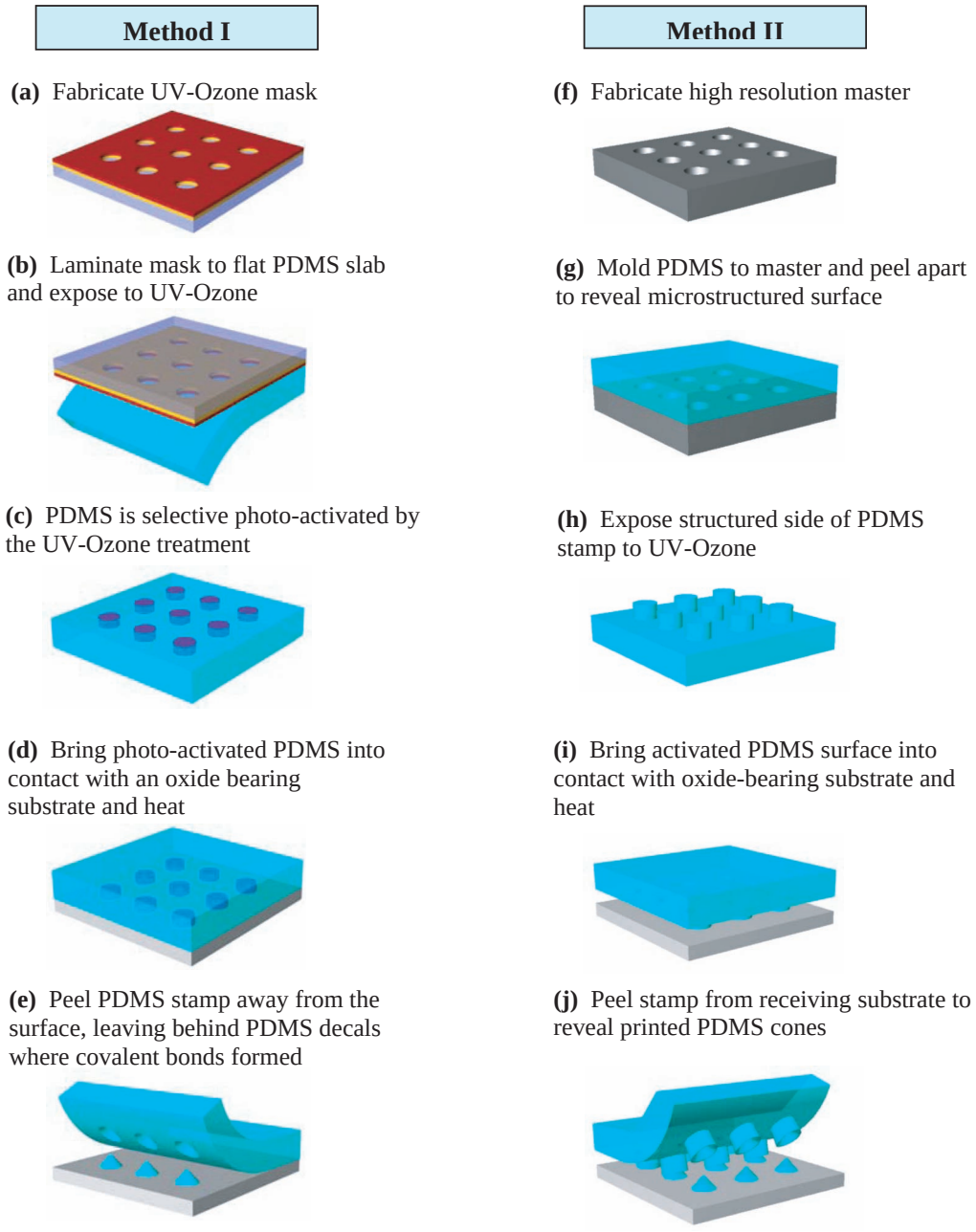

Figure 1. Schematic illustration of Method I (Left column). a) First a quartz-based UV-ozone microreactor mask is fabricated by patterning an opaque gold film by photolithography and etch-back. The photoresist is left on the surface of the patterned gold to increase the volume of the microreactor chambers. b) The mask is laminated onto the surface of a flat PDMS stamp, and then c) selective photoactivation of PDMS by UV-ozone treatment through the mask pattern. d) The photoactivated PDMS stamp is brought into contact with an oxide bearing surface. e) After heating, covalent bonds form between the activated regions of the PDMS stamp and the substrate. When the stamp is peeled away from the substrate surface, PDMS decals are left behind. When open circular holes are used to pattern the mask, cones result; open straight lines produce triangular prisms. Schematic illustration of Method II (Right column). f) First, a soft lithography master is fabricated to embody relief features of the desired pattern. g) PDMS is molded to this master, cured, and removed to reveal a micro- or nanostructured surface. h) The structured surface of the PDMS is exposed to UV-ozone, and then i) brought into contact with an oxide-bearing surface. j) After heating, covalent bonds form between the areas of the PDMS stamp in contact with the substrate; peeling the stamp away from the substrate leaves behind PDMS decals where the stamp was in contact. For stamps with cylindrical posts, cones result; stamps with rectangular channels print triangular prisms.

of any pattern configuration and a wide range of size scales can be used for this process, although cylindrical posts and rectilinear line patterns are typically used to produce features with triangular cross-sections. Figure 1f–j displays a schematic representation of the fabrication protocol.[34] The structured face of the PDMS stamp is flood exposed to UV-ozone, such that the entire surface is photo-activated. When brought into contact with an oxide bearing substrate, only the areas protruding from

the surface of the stamp make contact, and subsequently form strong adhesive bonds that allow PDMS decals to be printed when the stamp is peeled away. As before, conical decals result from cylindrical PDMS posts and triangular prisms result from stripes, with similar lateral resolution limits to those observed for Method I, although with smaller height to width aspect ratio of around 0.1. A compelling aspect of Method II is the inherent flexibility of using pre-existing masters to produce high resolution PDMS stamps, a quality that is especially important for patterns that require time-consuming and expensive serial fabrication processes.

The work presented in this paper exploits stamps fabricated by either Method I or II, using them in a variety of soft lithographic embossing schemes to transfer the corresponding patterns into application-enabling materials. The printed PDMS decals are also used in their native form, joined with thin film deposition processes, to enable a specific use in (plasmonically coupled) spectroscopic sensing. The demonstrated applications illustrate the utility of the PDMS decals for a wide range of optics-centric applications.

2.2. Near-Field Phase Shift Lithography

A number of reports document the successful fabrication of sub-100 nm features using PDMS phase masks in conjunction with conventional photoresists.[41–44] The PDMS masks used in essentially all forms of (soft) interference lithography are generally fabricated by soft lithographic replica molding. A master in the inverse form of the desired mask geometry is used as a mold, against which PDMS pre-polymer is cast and cured. On delamination, a mask bearing embossed PDMS features is obtained; this corrugation is used to modulate the phase of the dominant wavelength of light passing through the mask (λ = 365 nm). For an exposure through a mask with rectilinear relief features, the phase of the light is shifted by an amount determined by the depth of the relief and the index of refraction of the materials involved, in this case $n_{PDMS} \approx 1.43$ and $n_{air} \approx 1$.[41] If the phase mask features shift the phase of incident light by an odd multiple of π, destructive interference decreases the intensity to zero at the edges of the relief features.[42–44] The photoresist features resulting from phase shift lithography occur as a result of these nulls in intensity, the pattern pitch is therefore distributed accordingly and the width of the photoresist features dictated by the size of the dips in intensity. Rectangular mask design rules, however, are limited by the mechanical instabilities inherent to PDMS, experiencing feature sagging or pairing at low or high aspect ratios.[45]

Here we explore the use of elastomeric near field phase shift masks with triangular surface structures fabricated by Method I. The sloped profile of the phase mask elements result in a phase change that steadily decreases the incident light intensity to zero at the apex of the triangular feature; photoresist patterns with profiles that are also triangular in shape result, following forms where their smallest feature sizes approach zero-width. Furthermore, from a structural integrity standpoint, triangular cross sections provide a supported geometry that limits the instabilities that usually occur in high aspect ratio PDMS structures. The data presented here demonstrate that these optics, in terms of the model applications illustrated, behave comparably in terms of quality as other more conventional soft, near-field phase shift masks reported in the literature.

In order to provide a comparison between the soft lithography based Method I and traditional anisotropic wet etching of Si(100), each method was used to fabricate soft lithography masters containing triangular grooves. These results are presented in **Figure 2** and **Figure 3**. For these comparisons, the PDMS replicas formed from each master were used as near field phase shift lithography masks to pattern photoresist and finite element simulations (using Comsol Multiphysics) run to predict the intensity distribution of the light passing through the masks. The experimental results validated the predictions from the FEM model, thus allowing geometric design rules to be tested and optimized prior to experimental work.

As briefly described earlier, a Si(100) wafer was patterned with stripes of SiO_2 aligned slightly off-angle from the <110> direction. The exposed silicon was then etched in a heated KOH-based solution to preferentially etch the silicon along the <110> direction, resulting in lines of triangular pits with {111} sidewalls.[28,46] The intentional misalignment of the line pattern produces features with spaces between each groove; this feature spacing can be varied with the degree of offset. For the demonstration shown here, we selected a structure with horizontal spaces between each groove comparable to the types of features achieved by Method I. Fabrication of the phase mask proceeds by molding PDMS to the fabricated silicon master. A higher modulus PDMS, herein referred to as hard PDMS, was first spin-coated onto the surface of the master to provide a high fidelity but mechanically robust replica of the mask features. Next a thicker PDMS layer was added to form a soft backing that allows for mechanical flexibility and easier handling. The use of hard PDMS features supported on a lower modulus backing layer (herein referred to as a composite PDMS stamp) minimizes undesirable mechanical instabilities/sagging in the replicated masks.[47–54]

Figure 2a shows an AFM image and corresponding cross-sectional height profile of a composite PDMS phase mask with molded Si(100) triangular prisms with a width of 7.3 μm, height of 2.7 μm, and a 10 μm peak to peak separation distance. Figure 2b,c show AFM height images and corresponding height profiles of photoresists, negative and positive contrasts respectively, patterned with the mask shown in Figure 2a. Finite element modeling of the light (λ = 365 nm) intensity distribution through the mask in Figure 2a was carried out to predict the time averaged power flow at a distance 50 nm below the surface of the photoresist. Figure 2d shows the results of simulations for one unit cell of the phase mask cross section (left) as well as a representative time averaged power flow plot corresponding to the entire phase mask geometry shown in Figure 2a. The model's predictions correspond well to the experimental results; the model predicts that there is a sharp, high intensity peak located at the apex of the phase mask, along with a broader, less intense, peak attributed to the light passing through the region of horizontal recess. Additionally, a null in intensity occurs at the edge of each corner formed at the base of the triangular feature. As predicted by the model, the experimental results show that two main features of different width and height are transferred to the (negative and positive tone) photopatterned

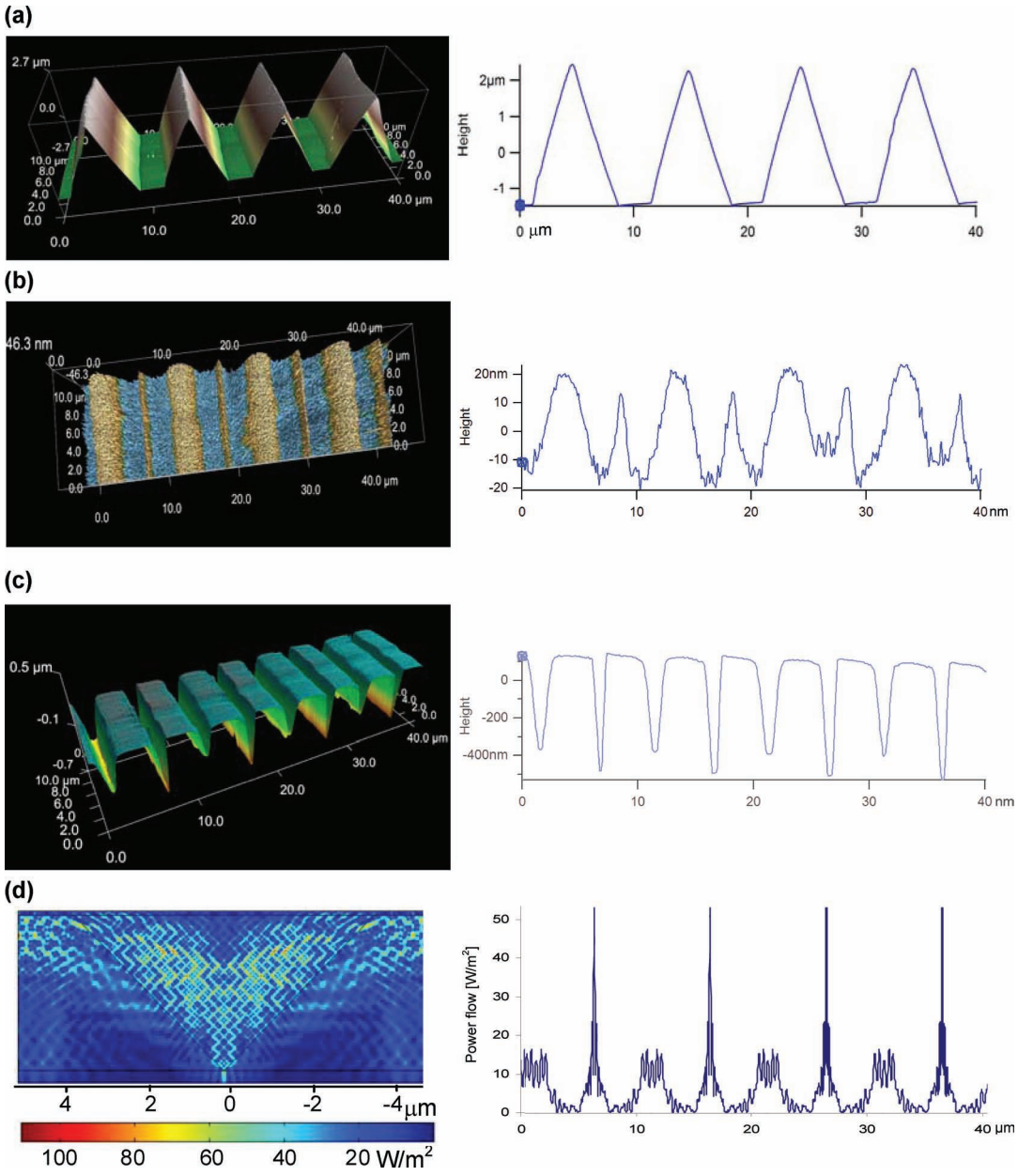

Figure 2. a) AFM height image (left) and corresponding line scan (right) of a composite PDMS phase mask molded from a soft lithography mask fabricated by anisotropic etching of Si(100). b) AFM height image (left) and corresponding height profile (right) of negative photoresist patterned with the mask shown in (a). c) AFM height image (left) and corresponding height profile (right) of positive photoresist patterned with the mask shown in (a). d) FEM calculation of the time averaged power flow through one unit cell of the mask shown in (a) (left), as well as a representative line profile corresponding to the portion of the mask shown in (a) (right).

polymers in registry to the emissive structures of each unit cell of the mask.

A complimentary composite PDMS stamp was patterned from a master fabricated by Method I. Figure 3a,b present SEM and AFM images of this triangular phase mask, one with a base width of 7 µm, height of 1.9 µm, and peak to peak periodicity of 10 µm. The mask was then used to expose AZ5214 photoresist by near-field phase shift lithography. Figure 3c presents a height profile of the patterned photoresist, here used as a negative photoresist, acquired from an area AFM scan. The peaks of the photoresist pattern correspond to the areas where the apex of the triangular mask elements make contact with the photoresist, providing a direct physical demonstration that the intensity of the transmitted light decreases gradually to zero along the sloped profile of the triangular cross section features. The time averaged power flow through the phase mask, as deduced from the COMSOL model, is shown in Figure 3d. A direct correlation between the trends in power flow predicted by the model and the experimental results is observed, with the undulations in power flow following in close agreement with the height profile

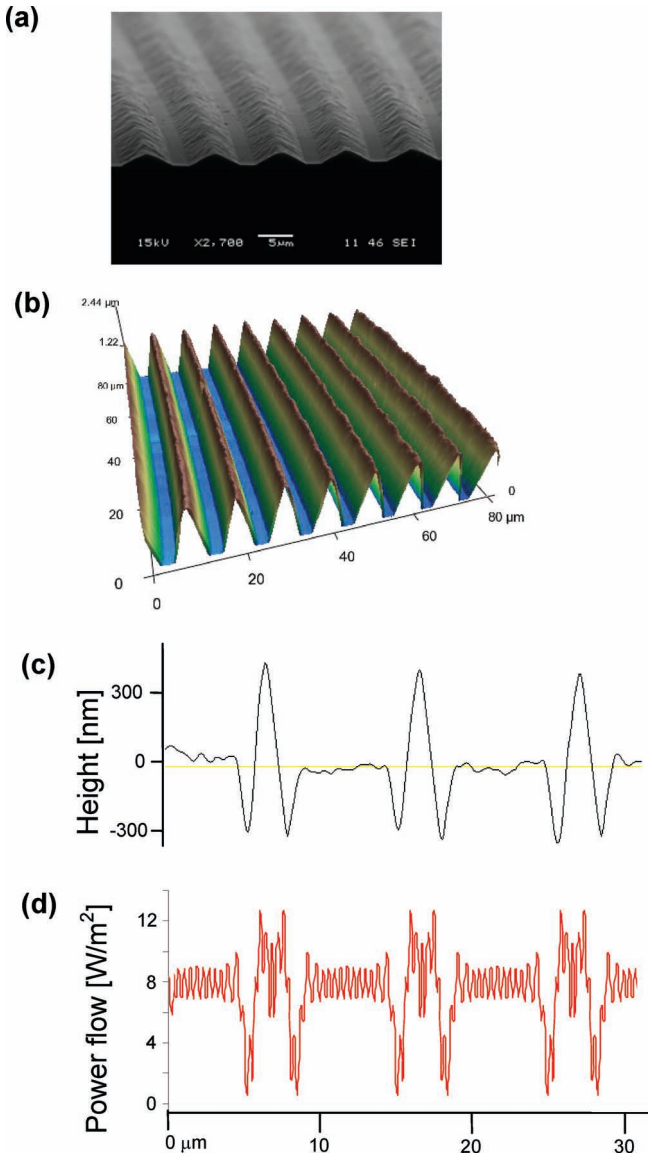

Figure 3. a) Angled SEM and b) AFM height profile of a composite hard/soft PDMS phase mask molded from a soft lithography master fabricated by Method I. The average full-scale feature height for the pillar-like crossing points of the component line patterns is ~700 nm. c) AFM line scan providing the height profile of negative photoresist patterned with the mask shown in (a) and (b). d) FEM computation of the light intensity distribution (measured by power flow) that results when photoresist is exposed through the mask shown in (a) and (b).

of the patterned photoresist. It is interesting to note that one predicted feature, namely the small dip in intensity at the apex of the triangle, is not resolved in the photoresist. This slight discrepancy between the model and experiment likely arises as a result of several contributing factors. First, we note the non-perfect geometry of the actual mask's cross-section relative to that of the ideal isosceles triangle geometry used to model the system (because of the means of fabrication used, the former is rougher and slightly asymmetric).[55] The largest contribution to the broadened intensity likely results from a slight compression of the tips of the triangular mask upon contact the hard, photoresist-coated, substrate.[56]

Previous studies in near field phase shift lithography have shown that the resulting intensity distributions strongly depend on the distance from the surface of the mask. In order to gain insight into the dependence of the vertical distance between the mask features and the surface of the photoresist, Method I was extended as a two-step additive printing process.[34] One set of triangular prismatic lines was first printed onto a receiving substrate and then a second set of identical lines, rotated 90° with respect to the first set, printed directly on top. The resulting structure, shown in **Figure 4**a, is a grid consisting of two sets of perpendicular overlapping lines. The regions where the two lines intersect have a height equal to the sum of the heights of the two comprising lines. This mask structure provides discrete areas of conformal contact, at the taller areas of line overlap, yet provide a supported structure that holds the mask at a constant

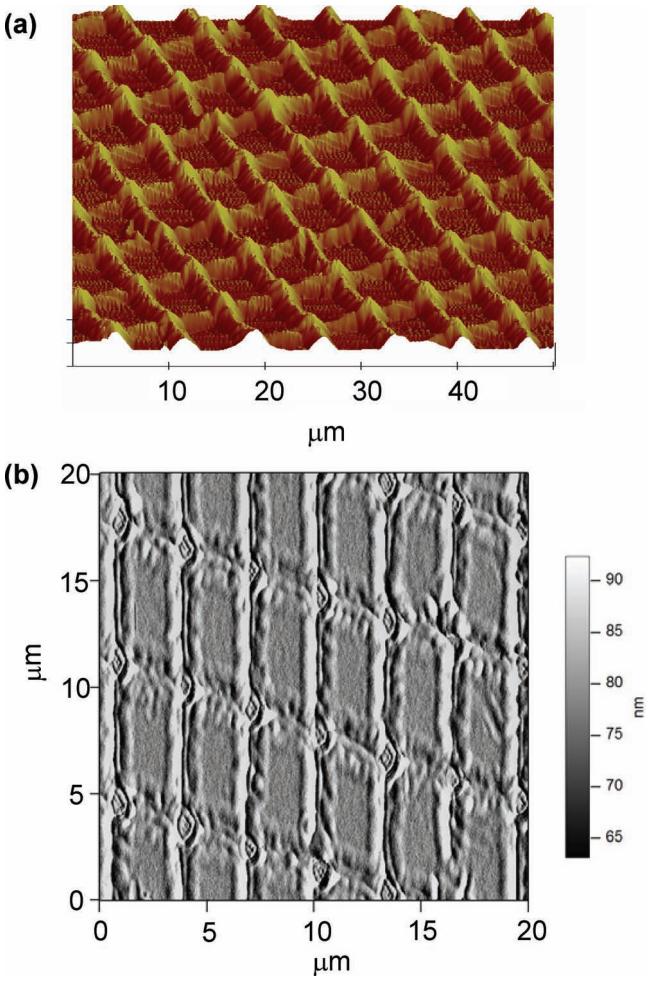

Figure 4. a) AFM image of a mask that was molded from a master fabricated using a two-step implementation of Method I, wherein PDMS lines are printed on SiO_2 and then the printing step is repeated with the printed lines rotated by 90°. The areas of overlap produce features that are 2× the height of the original individual line patterns due to the additive nature of the printing process. b) AFM image of positive photoresist exposed through the multi-height phase mask shown in (a).

distance from the substrate. Figure 4b presents a microscopy image of the photoresist pattern that resulted from exposure through the multi-height mask shown in Figure 4a. The FEM simulations made to characterize the light intensity distribution for the mask indicated that the areas in contact with the photoresist, in this case the areas of overlap in the mask, coincide with the maxima of the intensity distributions. The AFM image in Figure 4b illustrates that, as predicted by the model intensity distributions, the maximum exposure occurs at the intersections of the line resulting in the shortest feature heights. A discrete circular ring is also noticeable in the photoresist pattern, a feature similar to that reported for a double exposure performed using a rectilinear PDMS phase mask where the first and second exposures were rotated 90° relative to one another.[41] The other features of the mask, the prisms of constant height, are held 300 nm above the surface by the taller corner peaks. These triangular features experience a large difference in power flow between the local height maxima and minima of the mask elements. The corrugations of the developed photoresist pattern shown in Figure 4b confirm this prediction.

In addition to lines with characteristically triangular cross-sections, masks with conical features can also be fabricated using a means such as that of Method I (Figure 1). **Figure 5**a,b present SEM and AFM images, respectively, of composite PDMS phase masks molded from a master fabricated by Method I. The conical mask features shown in the figure are 5 μm in diameter and 1.4 μm tall, in accordance with the 0.3 height to width ratio observed for other features printed (for this modulus silicone) by Method I. Figure 5c shows the resulting light intensity distribution predicted by FEM for a conical mask. As expected, a peak in the power flow is observed at the apex of the cone, and the patterned positive photoresist closely corresponds to this predicted intensity profile, as shown in the images of Figure 5d,e. The features in the photoresist have been reduced in size to 1.8 μm relative to the original mask feature size of 5 μm, highlighting the important idea that photoresist feature sizes significantly smaller than those represented by the original mask can be realized. We note that it appears that the recessed spaces between the cones seem to provide two sub-micron scale features in the photoresist, but it is difficult to fully discriminate them from the overall roughness of the developed photoresist film.

It is evident that the masters fabricated by Method I produce effective near field phase shift lithography masks, with results comparable to those fabricated using a more traditional etched Si mastering protocol. The decal transfer lithography based fabrication approach, though, allows more flexibility as to accommodating mask designs (specifically in terms of pitch, spatial layout of the features, and geometric diversity). We emphasize the important implications of this work, mostly notably that features approaching zero-order widths can be obtained from micron-size-regime mask sets. Just as remarkable is the simple fabrication of multi-height mask features that provide a simple route to 3D photoresist patterns that would typically require specially designed high resolution grayscale lithography masks to fabricate. The ability to accurately compute the resulting photoresist structures is perhaps the most powerful attribute for efficient mask design, as it allows optimization of experimental variables through simulation instead of experiment.

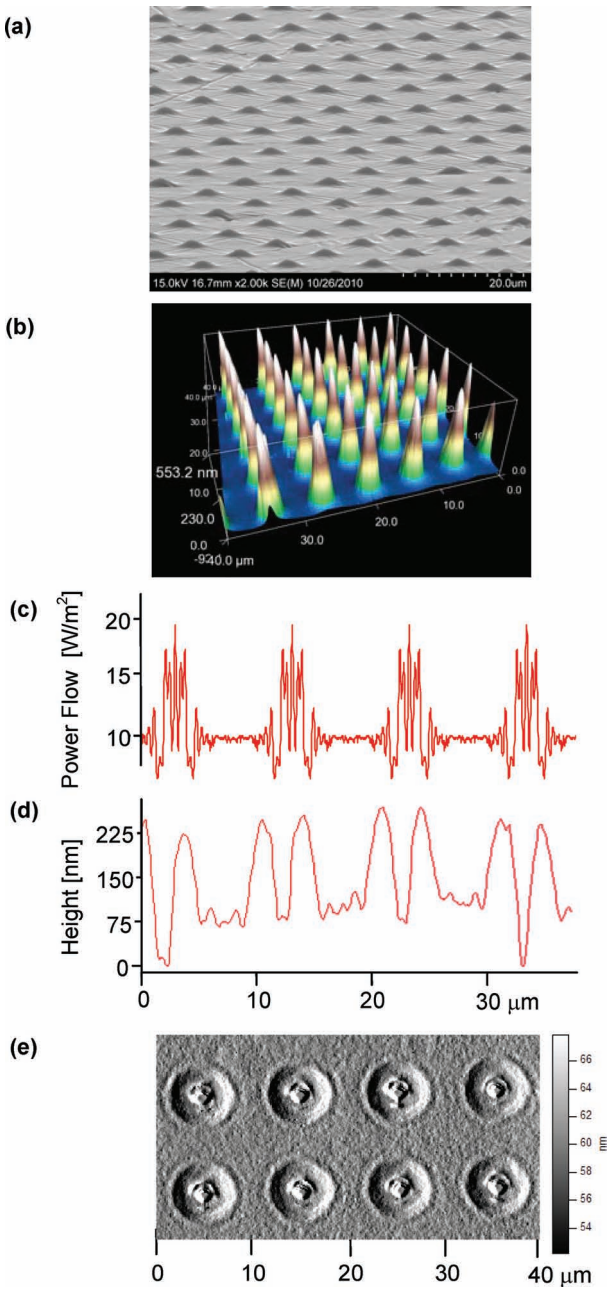

Figure 5. a) Angled SEM and b) AFM height profile of a composite hard/soft PDMS phase mask molded from a soft lithography master fabricated by Method I. c) FEM computation of the light intensity distribution (measured by power flow) that results when photoresist is exposed through the mask shown in (a) and (b). d) AFM line scan and e) image providing the height profile of positive photoresist patterned with the mask shown in (a) and (b). The *x*-axes of line scans in (c) and (d) are slightly offset. Minima in the resist height line scan correspond to regions of highest intensity in transmitted light predicted in the model. The resist resolution/processing conditions do not achieve pattern resolution sufficient to show the finer features predicted by FEM.

2.3. Maskless Proximity Field Nanopatterning

To demonstrate other light-mediated patterning capabilities, we examined a prototypical form of 3D interference lithography,

maskless proximity field nanopatterning (PnP).[57–60] The PnP method provides a facile means for imparting 3D nanoscale structures into the bulk of a photosensitive polymer. Maskless proximity field nanopatterning itself has been extensively studied and optimized, however the use of non-traditional diffraction grating pattern geometries has not been explored. We fabricated a composite PDMS stamp using a two step embossing scheme that provided a high resolution replica of conical PDMS decals (made by Method II). Nanoimprint lithography was used to emboss these conical relief features into the surface of a photoresist (in this case the epoxy-based SU-8). The samples were examined at each step of the embossing scheme by AFM, in order to verify that the fidelity of the stamp features was not comprised by the pattern replication process. **Figure 6**a presents an inverted AFM image of the resulting imprinted SU-8 photoresist; the AFM scan has been rotated 180° such that the relief feature pattern can be easily viewed and analyzed. The conical relief features closely reproduce those of the embossing tool. The topology, lateral size, depth, and pitch of the imprinted features dictate the properties of the diffraction grating that in turn generates the interference pattern within the photoresist during laser exposure. After selectively cross-linking those areas subject to the appropriate exposure dosage, and upon development, a 3D periodic polymer network is obtained.

The design rules for the grating were optimized through optical modeling by finite difference time domain (FDTD) methods. These simulations provide insights into the intensity distributions that result from these specific pattern geometries, as demonstrated by the results of the model shown in Figure 6b. It is evident from the resulting cross-sectional SEM image of the developed SU-8 photoresist (Figure 6c) that the simulation predicts the set of offset interconnections in the resist that is realized experimentally.

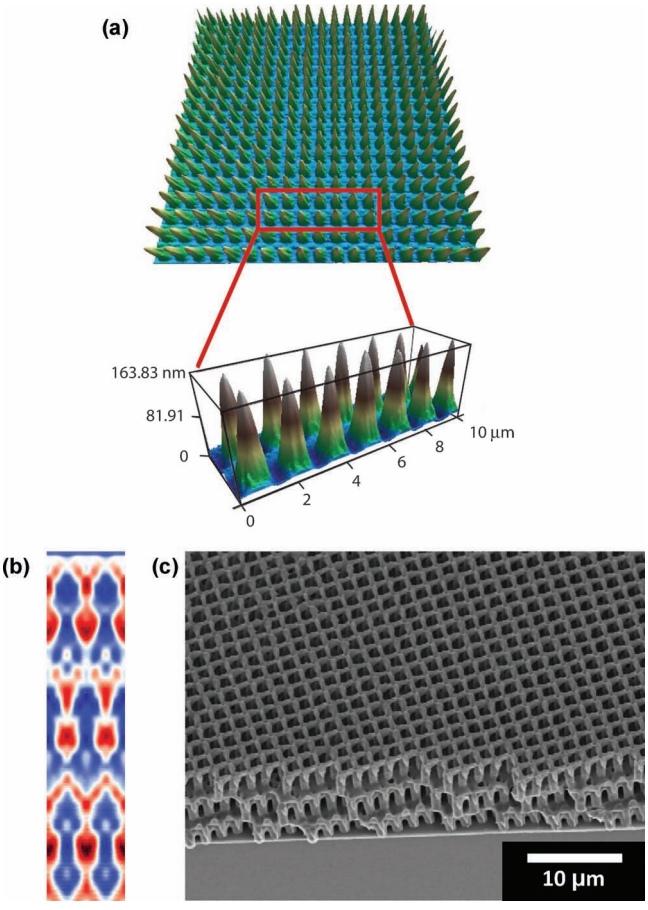

Figure 6. a) AFM height profile of SU-8 imprinted using a stamp patterned by Method II and a two-step embossing protocol. The AFM image has been inverted (rotated by 180°) for easier viewing of the topography of the relief features. b) FDTD simulation results predict the 3D periodic intensity distribution that results in the photoresist during maskless proximity field nanopatterning of the pattern shown in (a). c) Cross-sectional SEM image of SU-8 patterned by maskless PnP using the pattern shown in (a). This image shows that the conical pattern is compatible with the PnP process, and that three periods of the intended pattern have been achieved in the *z*-direction.

2.4. Embossed Inorganic Antireflective Coatings

To provide an exemplary application for the lithography enabled by these mastering protocols, a model 3D antireflective coating was fabricated. The surfaces of optical devices can be modified in this way using multi-layered thin film coatings of materials of varying refractive index or through texturing with a periodically structured array.[17] Tapered high aspect ratio structures provide the ideal geometry for anti-reflection, but are challenging to fabricate by traditional lithography.[61] Many approaches couple complex and time consuming fabrication schemes that generally utilize specialized lithography in tandem with etching protocols to impart the pattern directly into the surface of the device.[4,62] Specifically, electron-beam lithography and focused ion beam lithography have been employed to directly write structures, but are limited to small areas due to the time and capital intensive nature of these serial techniques. More efficient etch schemes, such as using a pre-made anodic porous alumina membrane as an etch mask,[63] or using a Bosch deep reactive ion etching process to nanostructure a silicon surface, often result in a randomized spatial layout and non-uniform feature heights, decreasing the efficacy of the antireflective coating. Nanoimprint lithographies offer a promising high-throughput approach to fabricating antireflective structures on materials surfaces, as it is quick, amenable to patterning on large area surfaces that have some topography, and shields the underlying substrate from the required use of harsh chemical etchants.[64–68] Imprint based approaches do, however, require the fabrication of a soft lithographic master, which must in turn be fabricated by a 3D lithography or replica embossing approach.[69] For the current demonstration, we fabricated square arrays of conical features (Method I), and subsequently used them as a soft-embossing tool for glass. By utilizing this embossing protocol, we show that it is possible to deliver high resolution antireflective structures to the surface of virtually any device.

In this demonstration, we used an inorganic spin-on-glass material[70–73] (SOG, Honeywell Spin-on-Glass 500F) as a thermoset thin film molded to take on the complimentary high resolution topography of the patterned stamp. The SOG is spin-coated directly onto the surface of the device (here a flat quartz substrate) and the PDMS stamp brought into contact with the

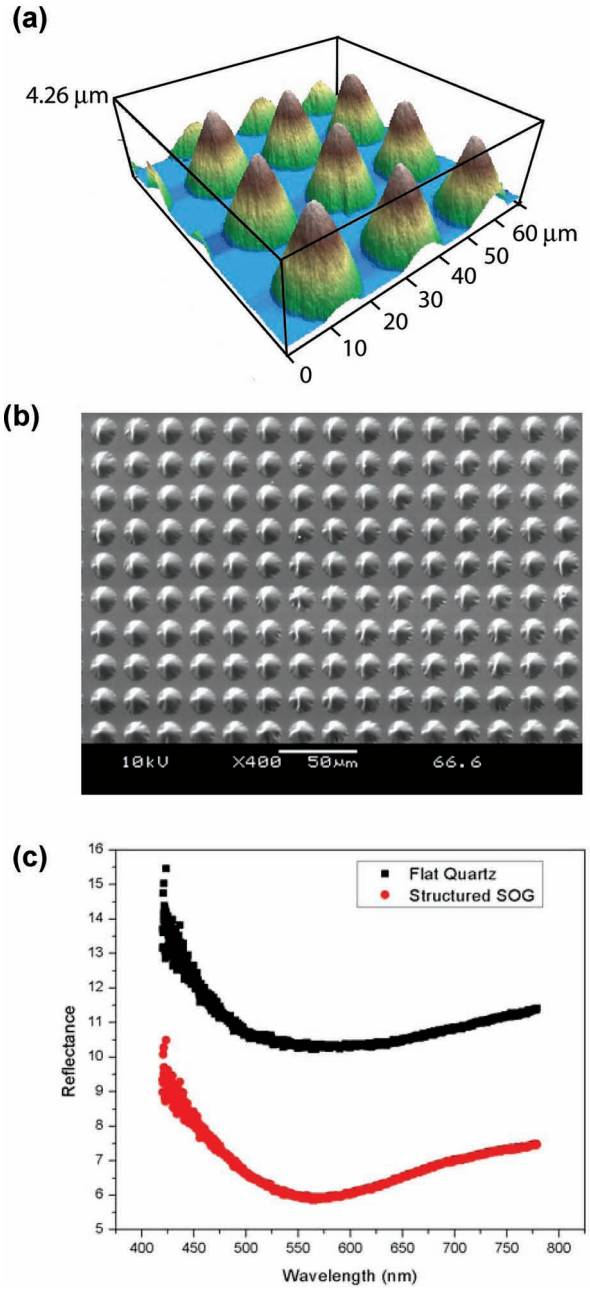

Figure 7. a) AFM height profile and b) top-down SEM image of the SOG film imprinted with cones using a PDMS stamp containing conical reliefs (20 µm diameter, 4.26 µm height, 2 µm edge to edge spacing) patterned by Method I. c) Near-normal reflection versus wavelength of a flat quartz substrate and the same quartz substrate microstructured with the SOG cone array shown in (a) and (b).

semi-liquid precursor. Heating steps are carried out to solidify the material, and upon removal of the stamp an embossed array of cones is obtained. **Figure 7**a shows the topography of the SOG cones, confirming that the shape follows closely to that of the PDMS decals. The top-view SEM image shown in Figure 7b shows that large pattern areas are achievable, one limited only by the scale of the decal transfer step used for the master.

The design rules of the textured coating were optimized by means of an FDTD simulation that predicted the anti-reflection performance of the SOG structures for different cone diameters, heights, and edge-to-edge spacings. Due to the roughly constant height to diameter aspect ratio produced by Method I, we found that larger, and therefore inherently taller, cones with minimal spacing provided the best performance, presumably due to scattering effects of the textured coating. As shown in Figures 7a,b, SOG cones with diameters of 20 µm were transferred to the surface of a flat quartz substrate, and the reflectance then measured normal to the surface for both a flat coated quartz slide and the same substrate patterned with the structured SOG. A significantly reduced reflectivity was observed on the structured SOG surface as compared to the flat quartz surface, as shown in Figure 7c, indicating that the coating provides the intended anti-reflection property. The optical model provided a guide for understanding the trends in how feature sizes correlate to coating performance. We found that the experiments did follow the trend predicted by the model, most notably that smaller features separated by a constant spacing embodied less effective antireflective properties than larger features separated by the same spacing.

The embossing method provides a route for delivering an antireflective coating to the surface of a device by simply spin coating the precursor material on the surface of the device and then embossing with a stamp containing the appropriate surface topography. Because PDMS is inert to many chemicals, a wide variety of materials that begin as a liquid precursor/prepolymer or that have T_g less than 150 °C can be embossed in this way. Above 150 °C PDMS begins to harden significantly, compromising its mechanical flexibility and ability to achieve good conformal contact with surfaces. This issue can be circumvented, however, by using other stamping materials that are able to withstand higher temperatures. The advantages of the method lie principally in its flexibility. Microstructures of useful gradient index form can be imprinted on a surface, without any etching, using a wide range of curable precursor materials in conjunction with low processing temperatures. We believe it will be possible to extend this method, with further improvements of the mastering protocols, to the fabrication of graded refractive index coatings embedding more challenging sub-wavelength feature sizes.

2.5. Fabrication of SERS Substrates for Detection of Organic Molecules

A major challenge in the fabrication of SERS-active optical substrates is the difficulty of producing uniform nanoscale patterns with demanding feature sizes over large areas. Design driven control over geometry is desirable, but in general is difficult to achieve with most fabrication methods. The fabrication of sensitive SERS substrates have been most commonly carried out using both etch based and stochastic additive (e.g., colloidal lithography) techniques. Serial writing techniques can provide high resolution features, but generally are not amenable to large area substrate patterning. Due to the inherent sensitivity of the resulting features to the processing conditions, it has been difficult to reproduce the geometries without significant sample to sample variations.[74–76]

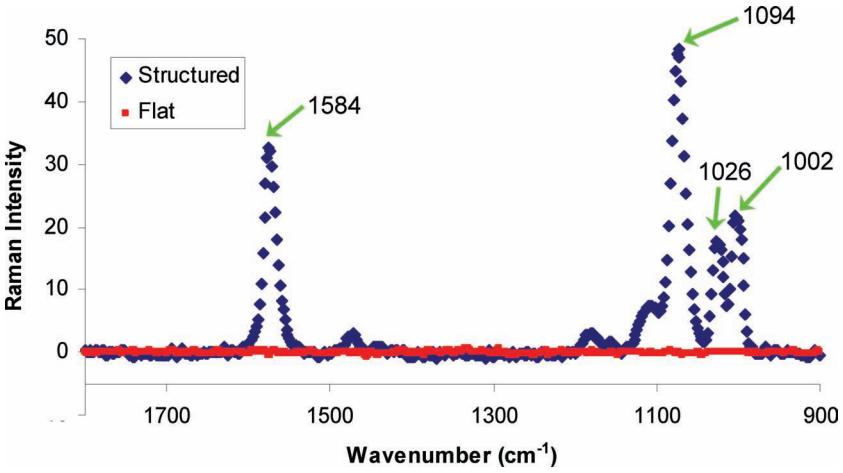

Figure 8. SERS spectrum of benzenethiol obtained from a quartz substrate patterned with PDMS cones, printed by Method II, then coated with SiO_2 and gold. The structured (cone array) substrate shows characteristic benezethiol peaks, while the flat substrate (quartz/SiO_2/gold) does not exhibit a detectable Raman signal. The green arrows indicate the main Raman-active vibrational modes for benzenethiol.[78]

We have found that printing PDMS cones by Method II provides a convenient and rapid fabrication approach to the preparation of SERS active substrates. The high resolution soft lithography master set used in Section 2.3 is one more generally useful for the fabrication of SERS active substrates. The masters for these samples were originally fabricated for imprinting nanostructured plasmonic crystals, therefore the existing design rules provided an ideal platform for fabrication of cones with sharp tips appropriate in size for SERS.[77] PDMS cones were printed on silica with the geometry and pitch shown in Figure 7a. The sample was then coated with a layer of SiO_2 and gold, and subjected to a solution phase deposition of benzenethiol in ethanol.

The Raman intensity plot presented in **Figure 8** shows data taken from the structured substrate along with a comparison to a flat substrate subjected to the same SiO_2, gold, and benzenethiol deposition conditions. It is evident that the flat substrate provides negligible signal, but that the structured surface shows features characteristic to benzenethiol as indicated by the close match between the experimentally acquired data and the main Raman-active vibrational modes (1002, 1026, 1094 and 1584 cm^{-1}) for benzenethiol.[78] This result suggests that the structured PDMS substrate provides a modest Raman signal enhancement with respect to the best validated enhancements which are on the order of 10^6–10^8,[78] albeit one still strong enough to detect a monolayer of benzenethiol. Further optimization of the size and pitch of the features are likely to further improve the enhancements of the Raman signal. The present data suggest embossing approaches may well provide a more broadly useful approach to the fabrication of SERS substrates.

3. Conclusions

Two decal transfer lithography based printing schemes were used to fabricate polymer-based soft lithography masters containing triangular features from which elastomeric stamps were replicated. These triangular stamps were then used for a variety of applications, focusing on exemplary cases requiring well-controlled light matter interactions. We demonstrate interference lithography techniques using the triangular stamps as masks, for both near-field and proximity-field approaches, to fabricate 3D periodic porous structures as well as photoresist features that approach zero-feature-width. Remarkably, the resolution of the near-field phase shift lithography patterns that result is significantly higher than the features on the mask itself, such that nanoscale patterns can be achieved using a micron-scale mask. The photoresist patterns are also shown to closely match FEM calculated predictions of the light intensity distribution passing through the mask during exposure. Triangular stamp designs are important for eliminating the need for more arduous fabrication techniques, such as e-beam writing and etch protocols that require extremely precise alignment. Large area patterns are also possible and two applications that benefit from the efficient processing are showcased in this work: fabrication of SERS substrates sensitive to a monolayer of an organic molecule, as well as the direct application of an embossed antireflective structure to the surface of an optical device. The demonstrated applications illustrate the utility of the triangular elastomeric stamps for a variety of well modeled optics-centric applications.

4. Experimental Section

Fabrication of Masters by Silicon Etching: A Si (100) wafer was cleaned with piranha solution (3:1 (v/v) mixture of sulfuric acid and hydrogen peroxide) for at least 30 min, rinsed with DI water (MilliQ), and finally dried with N_2. Next, 500 nm SiO_2 was grown on the surface of the Si by PECVD (PlasmaTherm/Unaxis SLR730). Photolithography was conducted using AZ 5214E photoresist (Clariant) to pattern the substrate with lines oriented approximately 2° off of the <110> direction. The exposed SiO_2 was then etched using buffered oxide etch solution, followed by photoresist lift-off in acetone, leaving behind the SiO_2 line pattern etch mask. Finally, the silicon was etched in a solution of Preferential Silicon Etchant (Transene PSE 200) heated to 100 °C for approximately 20 min. PSE etches along the <110> direction, resulting in triangular pits with {111} sidewalls. In order to prevent PDMS adhesion during the molding process, the surface of the patterned wafer was treated with (tridecafluoro-1,1,2,2-tetrahydrooctyl)trichlorosilane (No Stick, Gelest).

Fabrication of Masters by Method I: To fabricate UV-ozone masks, a quartz slide was first cleaned in a piranha solution for at least 30 min, rinsed thoroughly with DI water, and dried with N_2. Next, 5Å Ti and 1000Å Au were deposited by electron beam evaporation (Temescal FC-1800) onto the surface of the quartz, after which photolithography was used to pattern AZ 5214E photoresist. The patterned substrate was then subject to an O_2 plasma etch by RIE (50 mTorr, 10 sccm O_2, 150W, 30 s), and the exposed Au areas etched in a solution of TFA Gold Etch (Transene). The remaining photoresist was left as part of the final UV-ozone mask.

PDMS (Sylgard 184) pre-polymer was poured into a petri dish, degassed at 50 mTorr in a vacuum oven at room temperature for several minutes, and finally cured in an oven for 3 h at 70 °C. A scalpel was used to cut out the desired PDMS shape and size, and the stamp was separated from the dish. The flat PDMS slab was placed in conformal

contact with the patterned side of the UV-ozone mask (fabricated as above) and irradiated through the mask for 4 min at a distance less than 1 cm from the UV-ozone source (UVOCS T10 × 10). After exposure, the PDMS stamp was peeled away from the mask, and the patterned face of the stamp immediately placed into contact with an appropriate receiving substrate (in this case either a piranha cleaned Si wafer or glass microscope slide) and baked in an oven at 70 °C for at least 2 h. Finally, the PDMS stamp was carefully peeled from the receiving substrate to reveal a pattern of printed PDMS features corresponding to the open areas of the UV-ozone mask.

For multilayer patterns, a UV-ozone mask containing open lines was used to print PDMS decals on a receiving substrate, as described. The same UV-ozone mask was brought into contact with a second fresh PDMS slab and irradiated for 4 min, as before. This patterned stamp was then optically aligned directly on top of the first set of lines such that the line patterns were oriented perpendicular to each other. Once the PDMS stamp and receiving substrate were brought into intimate contact, the sample was heated at 140 °C for at least 1 h to promote formation of PDMS-PDMS bonds. Carefully peeling the stamp from the substrate revealed a second set of printed lines on top of the first.

Fabrication of Masters by Method II: A high resolution master, in this case one that was previously fabricated by e-beam lithography, was used to define the topography of a PDMS (Sylgard 184) stamp. PDMS pre-polymer was caste on the surface of the master, then degassed at 50 mTorr for several minutes, and finally cured in an oven for 3 h at 70 °C. After carefully cutting the stamp out with a blade and carefully separating it from the master, the patterned face of a molded PDMS stamp was exposed to UV-ozone for 3 min, then immediately placed in conformal contact with a receiving substrate and heated in an oven at 70 °C for at least 2 h. As before, the stamp was then peeled slowly away from the receiving substrate, printing PDMS decals in the areas where the stamp made contact.

Fabrication of Composite PDMS Stamps: For the work here, either the printed PDMS decals fabricated by Method I or II are used, or a bulk stamp containing relief features corresponding to the PDMS decals printed by Method I are used as soft lithography masters. For high resolution features, it is necessary to preserve pattern fidelity by fabricating composite PDMS stamps made of a thin layer of hard PDMS and backed with soft PDMS (Sylgard 184). Composite stamps in this paper were fabricated according to the protocol described by Odom et al.[47]

Patterning Photoresist by Near-Field Phase Shift Lithography: Two photoresists, AZ 5214E and S1805, were patterned by near-field phase shift lithography using a composite stamp, molded from a master fabricated by Method I, as the phase mask. S1805 was spin-coated onto a Si wafer at 3000 rpm for 30 s, which was then pre-baked at 115 °C for 3 min. The composite PDMS phase mask was brought into contact with the photoresist during a 2 s exposure using a Karl Suss MJB-3 mask aligner (light intensity ≈ 10 mW/cm^2). Finally, the pattern was developed using AZ MIF-319 developer solution. AZ5214E photoresist was patterned in image reversal mode, such that it would act as a negative resist. First, the resist was spin-coated at 4000 rpm for 30 s onto a Si wafer, followed by a soft bake of 90 °C for 40 s. Next, the phase mask was brought in contact and the resist was exposed through the mask for 5 s (light intensity ≈ 10 mW/cm^2). A 1 min post bake at 100 °C removed the acidic regions formed during the first exposure, and finally the sample was subject to a second 10 s flood exposure without the phase mask and developed in a 2:1 (v/v) AZ developer/water solution.

Finite Element Modeling: Details of the theory supporting the calculations performed in this work have been reported elsewhere.[79] All simulations were solved by the finite element method using COMSOL Multiphysics software. The masks were approximated by the closest ideal geometry; the triangular prism masks were modeled in 2D using the dimensions of the resulting triangular cross-section and assuming infinite length, while the cones were modeled in 3D based on a discrete idealized cone. The incident wavelength was set to 365 nm with an exposure intensity of 10 mW/cm^2 to approximate the properties of the mask aligner. The photoresist thickness was fixed at 300 nm with a back surface set to an impedance matched surface of silicon. The mesh size varied between two and ten elements per wavelength; the smallest possible mesh size was used, the size was determined by the total size of the geometry being modeled as well as the limitations of the available computing power.

Maskless Proximity Field Nanopatterning: A composite stamp fabricated from a master made by Method II was used to imprint a film of SU-8 photoresist. First, SU-8 2010 (MicroChem) was spin coated onto a clean glass slide at 3000 rpm for 30 s and pre-baked at 65 °C for 10 min then 95 °C for 25 min. Next, 2 drops of ethanol were deposited on the film to soften the SU-8, and the composite stamp was brought into contact with the photoresist under weight (~20 g) at room temperature for at least 1 h. Removal of the stamp reveals an imprinted relief pattern in the SU-8 that corresponds to the topography of the stamp.

The imprinted SU-8 film was then exposed using a regeneratively amplified cryogenically cooled Ti:sapphire laser operating at 1 KHz with FWHM pulsewidth of 7 nm/120 fs, $\lambda = 770$ nm, exposure power of 2 W, and 2.5 mm diameter beam. After exposure, the sample was post-baked at 95 °C for 60 s on a hotplate. Finally, the pattern was developed in propylene glycol monomethyl ether acetate (PGMEA) for 1 h and rinsed in a bath of IPA for 5 min to reveal the periodic porous pattern.

Imprinting Spin-On-Glass: Method I was used to print conical PDMS decals from a PDMS stamp, as described above. After printing, the PDMS stamp containing conical relief features was subject first to UV-ozone for 3 min, immediately followed by vapor-phase deposition of No-Stick accomplished by placing the PDMS stamp in an enclosed container with two drops of the No-Stick solution for 1 h. Next, spin-on-glass (SOG 500F, Honeywell) was filtered through a 0.2 mm syringe filter. 10 drops of the filtered SOG were directly deposited onto the surface of a quartz slide and spin coated at 600 rpm for 8 s. The PDMS stamp was immediately laminated onto the surface of the SOG coated quartz under weight for 1 hour at room temperature and then placed on a hotplate for 5 min at 110 °C. The stamp was carefully peeled off of the surface, after which the sample was heated for 5 min at 200 °C on a hotplate, and finally baked in an oven for 8 h at 160 °C then 1 h at 450 °C.

Sample Characterization: Atomic force microscopy (AFM; Asylum) images were taken on either a Digital Instruments Dimension 3100 operating in tapping mode or AC mode with an Asylum MFP-3D. AFM data was processed using V5.12r2 software (Digital Instruments) or Igor software, respectively. Scanning electron microscopy (SEM) was conducted using a Hitachi 4800. Reflectance measurements were performed using a Zeiss Axio Observer D1 inverted microscope and a CCD thermoelectrically cooled high-sensitivity spectrometer (420–780 nm). SERS spectra were collected with a Nicolet Almega XR Dispersive Raman microscope (Thermo Electron Corp. Madison, WI) using a 785 nm excitation laser; a 50 μm pinhole was used as the spectrograph aperture.

Acknowledgements

The authors would like to thank Tom Galvin and Prof. J. Gary Eden (ECE, UIUC) for assistance with and use of their laser. A.M.B. and J.M.L. were supported by the Light-Matter Interactions in Energy Conversion Energy Frontier Research Center (LMI-EFRC), an Energy Frontier Research Center funded by the U.S. Department of Energy, Office of Science, Office of Basic Energy Sciences under Award Number DE-SC0001293. A.J.B. would like to acknowledge Lee Cambrea and the ONR-IAR program for support. A.M. would like to thank the Beckman Institute for support through a postdoctoral fellowship. This work was carried out in part in the Frederick Seitz Materials Research Laboratory Central Facilities, University of Illinois at Urbana-Champaign, which are partially supported by the U.S. Department of Energy under grants DE-FG02-07ER46453 and DE-FG02-07ER46471.

Received: October 11, 2011
Revised: January 23, 2012
Published online: April 12, 2012

[1] S. Y. Chou, P. R. Krauss, P. J. Renstrom, *Appl. Phys. Lett.* **1995**, *67*, 3114.
[2] L. J. Guo, *Adv. Mater.* **2007**, *19*, 495.
[3] X. Zhang, J. Zhang, Z. Ren, X. Li, X. Zhang, D. Zhu, T. Wang, T. Tian, B. Yang, *Langmuir* **2009**, *25*, 7375.
[4] Y. Li, J. Zhang, B. Yang, *Nano Today* **2010**, *5*, 117.
[5] E. A. Dobisz, C. R. K. Marrian, *Appl. Phys. Lett.* **1991**, *58*, 2526.
[6] B. D. Terris, H. J. Mamin, M. E. Best, J. A. Logan, D. Rugar, S. A. Rishton, *Appl. Phys. Lett.* **1996**, *69*, 4262.
[7] Z. Liu, D. G. Bucknall, M. G. Allen, *Nanotechnology* **2011**, *22*, 225302.
[8] L. Miccio, M. Paturzo, A. Finizio, P. Ferraro, *Opt. Express* **2010**, *18*, 10947.
[9] M.-H. Wu, C. Park, G. M. Whitesides, *J. Colloid Interface Sci.* **2003**, *265*, 304.
[10] Y. S. Kim, K. Y. Suh, H. H. Lee, *Appl. Phys. Lett.* **2001**, *79*, 2285.
[11] H. Dang, J. L.-P. Tan, M. W. Horn, *J. Vac. Sci. Technol. B* **2003**, *21*, 1143.
[12] D. V. Gough, A. T. Juhl, P. V. Braun, *Mater. Today* **2009**, *12*, 28.
[13] J. Park, S. Yoon, K. Kang, S. Jeon, *Small* **2010**, *6*, 1981.
[14] J. Park, D.-H. Kim, G. Kim, Y. Kim, E. Choi, A. Levchenko, *Lab Chip* **2010**, *10*, 2130.
[15] H. Sato, S. Ito, K. Tajima, N. Orimoto, S. Shoji, *Sens. Actuators A* **2005**, *119*, 365.
[16] C. J. Evans, J. B. Bryan, *CIRP Ann. Manuf. Tech.* **1999**, *48*, 541.
[17] S. Chattopadhyay, Y. F. Huang, Y. J. Jen, A. Ganguly, K. H. Chen, L. C. Chen, *Mat. Sci. Eng. R* **2010**, *69*, 1.
[18] Z. Zheng, O. Azzaroni, F. Zhou, W. T. S. Huck, *J. Am. Chem. Soc.* **2006**, *128*, 7730.
[19] S.-G. Park, S. Y. Lee, S. G. Jang, S.-M. Yang, *Langmuir* **2010**, *26*, 5295.
[20] S.-J. Choi, S.-Y. Huh, *Macromol. Rapid Commun.* **2010**, *31*, 539.
[21] S. Lal, S. Link, N. J. Halas, *Nat. Photonics* **2007**, *1*, 641.
[22] K. Kneipp, *Phys. Today* **2007**, *60*, 40.
[23] D. Wouters, U. S. Schubert, *Angew. Chem. Int. Ed.* **2004**, *43*, 2480.
[24] B. D. Gates, Q. Xu, M. Stewart, D. Ryan, C. G. Wilson, G. M. Whitesides, *Chem. Rev.* **2005**, *105*, 1171.
[25] V. P. Chuang, J. Y. Cheng, T. A. Savas, C. A. Ross, *Nano Lett.* **2006**, *6*, 2332.
[26] G. Willeke, H. Nussbaumer, H. Bender, E. Bucher, *Sol. Energy Mater. Sol. C.* **1992**, *26*, 345.
[27] K. E. Petersen, *Proc. IEEE* **1982**, *70*, 420.
[28] K. B. Bean, *IEEE Trans. Electron. Dev.* **1978**, *25*, 1185.
[29] K. Khare, J. Zhou, S. Yang, *Langmuir* **2009**, *25*, 12794.
[30] J. Genzer, J. Groenewold, *Soft Matter* **2006**, *2*, 310.
[31] S. Yang, K. Khare, P.-C. Lin, *Adv. Funct. Mater.* **2010**, *20*, 2550.
[32] D. Huh, K. L. Mills, X. Zhu, M. A. Burns, M. D. Thouless, S. Takayama, *Nat. Mater.* **2007**, *6*, 424.
[33] M. T. Russell, L. S. C. Pingree, M. C. Hersam, T. J. Marks, *Langmuir* **2006**, *22*, 6712.
[34] W. R. Childs, M. J. Motala, K. J. Lee, R. G. Nuzzo, *Langmuir* **2005**, *21*, 10096.
[35] W. R. Childs, R. G. Nuzzo, *J. Am. Chem. Soc.* **2002**, *124*, 13583.
[36] Y. Xia, G. M. Whitesides, *Angew. Chem. Int. Ed.* **1998**, *37*, 550.
[37] J. A. Rogers, R. G. Nuzzo, *Mater. Today* **2005**, *8*, 50.
[38] J. Yao, A.-P. Le, S. K. Gray, J. S. Moore, J. A. Rogers, R. G. Nuzzo, *Adv. Mater.* **2010**, *22*, 1102.
[39] M. E. Stewart, N. H. Mack, V. Malyarchuk, J. A. N. T. Soares, T.-W. Lee, S. K. Gray, R. G. Nuzzo, J. A. Rogers, *Proc. Natl. Acad. Sci. USA* **2006**, *103*, 17143.
[40] M. E. Stewart, J. Yao, J. Maria, S. K. Gray, J. A. Rogers, R. G. Nuzzo, *Anal. Chem.* **2009**, *81*, 5980.
[41] J. Maria, S. Jeon, J. A. Rogers, *J. Photochem. Photobiol. A* **2004**, *166*, 149.
[42] J. A. Rogers, K. E. Paul, R. J. Jackman, G. M. Whitesides, *Appl. Phys. Lett.* **1997**, *70*, 2658.
[43] J. A. Rogers, K. E. Paul, R. J. Jackman, G. M. Whitesides, *J. Vac. Sci. Technol. B* **1998**, *16*, 59.
[44] J. Aizenberg, J. A. Rogers, K. E. Paul, G. M. Whitesides, *Appl. Phys. Lett.* **1997**, *71*, 3773.
[45] E. Delamarche, H. Schmid, B. Michel, H. Biebuyck, *Adv. Mater.* **1997**, *9*, 741.
[46] W.-H. Chang, Y.-C. Huang, *Microsys. Technol.* **2005**, *11*, 117.
[47] T. W. Odom, J. C. Love, D. B. Wolfe, K. E. Paul, G. M. Whitesides, *Langmuir* **2002**, *18*, 5314.
[48] B. D. Gates, G. M. Whitesides, *J. Am. Chem. Soc.* **2003**, *125*, 14986.
[49] H. Schmid, B. Michel, *Macromolecules* **2000**, *33*, 3042.
[50] V. Malyarchuk, F. Hua, N. H. Mack, V. T. Velasquez, J. O. White, R. G. Nuzzo, J. A. Rogers, *Opt. Express* **2005**, *13*, 5669.
[51] M. M. J. Decre, P. H. M. Timmermans, O. van de rSluis, R. Schroeders, *Langmuir* **2005**, *21*, 7971.
[52] C. Y. Hui, A. Jagota, Y. Y. Lin, E. J. Kramer, *Langmuir* **2002**, *18*, 1394.
[53] K. G. Sharp, G. S. Blackman, N. J. Glassmaker, A. Jagota, C. Y. Hui, *Langmuir* **2004**, *20*, 6430.
[54] W. Zhou, Y. Huang, E. Menard, N. R. Aluru, J. A. Rogers, A. G. Alleyne, *Appl. Phys. Lett.* **2005**, *87*, 251925.
[55] G. Kostovski, A. Mitchell, A. Holland, E. Fardin, M. Austin, *Appl. Phys. Lett.* **2006**, *88*, 133128.
[56] C. Y. Hui, Y. Y. Lin, J. M. Baney, E. J. Kramer, *J. Polym. Sci. Polym. Phys.* **2001**, *39*, 1195.
[57] M. C. George, E. C. Nelson, J. A. Rogers, P. V. Braun, *Angew. Chem. Int. Ed.* **2008**, *121*, 150.
[58] D. Shir, H. Liao, S. Jeon, D. Xiao, H. T. Johnson, G. R. Bogart, K. H. A. Bogart, J. A. Rogers, *Nano Lett.* **2008**, *8*, 2236.
[59] D. Shir, E. C. Nelson, Y. C. Chen, A. Brzezinski, H. Liao, P. V. Braun, P. Wiltzius, K. H. A. Bogart, J. A. Rogers, *Appl. Phys. Lett.* **2009**, *94*, 01 1101.
[60] S. Jeon, D. J. Shir, Y. S. Nam, R. Nidetz, M. Highland, D. G. Cahill, J. A. Rogers, M. F. Su, I. F. El-Kady, C. G. Christodoulou, G. R. Bogart, *Opt. Express* **2007**, *15*, 6358.
[61] S. A. Boden, D. M. Bagnall, *Prog. Photovoltaics* **2010**, *18*, 195.
[62] K. Yamada, M. Umetani, T. Tamura, Y. Tanaka, H. Kasa, J. Nishii, *Appl. Surf. Sci.* **2009**, *255*, 4267.
[63] K. Choi, S. H. Park, Y. M. Song, Y. T. Lee, C. K. Hwangbo, H. Yang, H. S. Lee, *Adv. Mater.* **2010**, *22*, 3713.
[64] Q. Chen, G. Hubbard, P. A. Shields, C. Liu, D. W. E. Allsopp, W. N. Wang, S. Abbott, *Appl. Phys. Lett.* **2009**, *94*, 263118.
[65] Z. Yu, H. Gao, W. Wu, H. Ge, S. Y. Chou, *J. Vac. Sci. Technol. B* **2003**, *21*, 2874.
[66] K.-Y. Yang, K.-S. Han, H. Lee, *J. Electrochem. Soc.* **2011**, *158*, K141.
[67] K. Sogo, M. Nakajima, H. Kawata, Y. Hirai, *Microelectron. Eng.* **2007**, *84*, 909.
[68] K.-S. Han, J.-H. Shin, W.-Y. Yoon, H. Lee, *Sol. Energ. Mater. Sol. C* **2011**, *95*, 288.
[69] T.-I. Kim, J.-H. Kim, S. J. Son, S.-M. Seo, *Nanotechnology* **2008**, *19*, 295302.
[70] P. K. Biswas, D. Kundu, D. Ganguli, *J. Mater. Sci. Lett.* **1989**, *8*, 1436.
[71] C. J. Brinker, M. S. Harrington, *Sol. Energy Mater.* **1981**, *5*, 159.
[72] W. Zhou, M. Tao, L. Chen, H. Yang, *J. Appl. Phys.* **2007**, *102*, 103105.
[73] X. Wang, J. Shen, *J. Sol-Gel Sci. Technol.* **2010**, *53*, 322.
[74] M. S. Schmidt, A. Boisen, J. Hubner, *IEEE Sens. J.* **2009**, 1763.
[75] W. Wu, M. Hu, F. S. Ou, Z. Li, R. S. Williams, *Nanotechnology* **2010**, *21*, 255502.
[76] Y. Yang, M. Tanemura, Z. Huang, D. Jiang, Z.-Y. Li, Y.-P. Huang, G. Kawamura, K. Yamaguchi, M. Nogami, *Nanotechnology* **2010**, *21*, 325701.
[77] G. A. Baker, D. S. Moore, *Anal. Bioanal. Chem.* **2005**, *382*, 1751.
[78] S. K. Saikin, Y. Chu, D. Rappoport, K. B. Crozier, A. Aspuru-Guzik, *J. Phys. Chem. Lett.* **2010**, *1*, 2740.
[79] J. Maria, V. Malyarchuk, J. White, J. A. Rogers, *J. Vac. Sci. Technol. B* **2006**, *24*, 828.